p16INK4a deficiency promotes IL-4-induced polarization and inhibits proinflammatory signaling in macrophages.

Céline Cudejko, Kristiaan Wouters, Lucía Fuentes, Sarah Anissa Hannou, Charlotte Paquet, Kadiombo Bantubungi, Emmanuel Bouchaert, Jonathan Vanhoutte, Sébastien Fleury, Patrick Remy, et al.

▶ **To cite this version:**

Céline Cudejko, Kristiaan Wouters, Lucía Fuentes, Sarah Anissa Hannou, Charlotte Paquet, et al.. p16INK4a deficiency promotes IL-4-induced polarization and inhibits proinflammatory signaling in macrophages.: p16INK4a function in macrophages. Blood, 2011, 118 (9), pp.2556-66. 10.1182/blood-2010-10-313106 . inserm-00605106

HAL Id: inserm-00605106
https://inserm.hal.science/inserm-00605106

Submitted on 30 Jun 2011

HAL is a multi-disciplinary open access archive for the deposit and dissemination of scientific research documents, whether they are published or not. The documents may come from teaching and research institutions in France or abroad, or from public or private research centers.

L'archive ouverte pluridisciplinaire **HAL**, est destinée au dépôt et à la diffusion de documents scientifiques de niveau recherche, publiés ou non, émanant des établissements d'enseignement et de recherche français ou étrangers, des laboratoires publics ou privés.

p16^{INK4a}-deficiency promotes IL-4-induced polarization and inhibits pro-inflammatory signaling in macrophages

Céline CUDEJKO[1,2,3,4,†], Kristiaan WOUTERS[1,2,3,4,†], Lucía FUENTES[1,2,3,4], Sarah Anissa HANNOU[1,2,3,4], Charlotte PAQUET[1,2,3,4], Kadiombo BANTUBUNGI[1,2,3,4], Emmanuel BOUCHAERT[1,2,3,4], Jonathan VANHOUTTE[1,2,3,4], Sébastien FLEURY[1,2,3,4], Patrick REMY[4,5], Anne TAILLEUX[1,2,3,4], Giulia CHINETTI[1,2,3,4], David DOMBROWICZ[1,2,3,4], Bart STAELS[1,2,3,4,*] and Réjane PAUMELLE[1,2,3,4].

1 Univ. Lille Nord de France, F-59000, Lille, France

2 Inserm, U1011, F-59000, Lille, France

3 UDSL, F-59000, Lille, France

4 Institut Pasteur de Lille, F-59019, Lille, France

5 Service de Production des antigènes, Institut Pasteur de Lille, F-59019, Lille, France

Short title: p16^{INK4a} function in macrophages

* Corresponding author: Bart Staels, Inserm UR 1011, Institut Pasteur de Lille, 1 rue du Professeur Calmette, BP 245, Lille 59019, France, Tel: +33 3 20 87 73 88, Fax: +33 3 20 87 73 60, E-mail: bart.staels@pasteur-lille.fr

† These authors contributed equally to this work.

Word count: 4900

Abstract count: 196

Figure count: 7 (and 10 Supplemental Figures)

Table count: 2 (and 4 Supplemental Tables)

Reference count: 50

ABSTRACT

The *CDKN2A* locus, which contains the tumor suppressor gene $p16^{INK4a}$, is associated with an increased risk of age-related inflammatory diseases, such as cardiovascular disease and type 2 diabetes, in which macrophages play a crucial role. Monocytes can polarize towards classically (CAMϕ) or alternatively (AAMϕ) activated macrophages. However, the molecular mechanisms underlying the acquisition of these phenotypes are not well defined.

Here, we show that $p16^{INK4a}$-deficiency ($p16^{-/-}$) modulates the macrophage phenotype. Transcriptome analysis revealed that $p16^{-/-}$ bone marrow-derived macrophages (BMDM) exhibit a phenotype resembling interleukin (IL)-4-induced macrophage polarization. In line with this observation, $p16^{-/-}$ BMDM displayed a decreased response to classically polarizing IFNγ and LPS and an increased sensitivity to alternative polarization by IL-4. Furthermore, mice transplanted with $p16^{-/-}$ bone marrow displayed higher hepatic AAMϕ marker expression levels upon *Schistosoma mansoni* infection, an *in vivo* model of AAMϕ phenotype-skewing. Surprisingly, $p16^{-/-}$ BMDM did not display increased IL-4-induced STAT6 signaling, but decreased IFNγ-induced STAT1 and LPS-induced IKKα,β phosphorylation. This decrease correlated with decreased JAK2 phosphorylation and with higher levels of inhibitory acetylation of STAT1 and IKKα,β. These findings identify $p16^{INK4a}$ as a modulator of macrophage activation and polarization via the JAK2-STAT1 pathway with possible roles in inflammatory diseases.

INTRODUCTION

The tumor suppressor $p16^{INK4a}$ is encoded by the *CDKN2A* locus on the human chromosome 9p21 and on the murine chromosome 4. $p16^{INK4a}$ belongs to the INK4 family of cyclin-dependent kinase (CDK) inhibitors, also including $p15^{INK4b}$, $p18^{INK4c}$, and $p19^{INK4d}$ [1-5]. $p16^{INK4a}$ inhibits cell cycle progression by preventing cyclin D-CDK 4/6 complex formation. As a consequence, pRb hyperphosphorylation and its association with E2F, which induces transcription of S phase genes, are inhibited. $p16^{INK4a}$ inactivation by deletion, point mutation or promoter methylation, occurs frequently in most tumors [6].

Besides its role in cancer as an inhibitor of cell cycle progression, $p16^{INK4a}$ plays a crucial role in senescence and aging [7, 8]. Indeed, expression of $p16^{INK4a}$ increases with age in various tissues from several species [9, -11]. A genome-wide association study has shown association of the *CDKN2A* locus with an increased risk of the age-related frailty syndrome [12]. Additionally, increased $p16^{INK4a}$ expression causes the age-dependent decline in proliferation of self-renewing cellular compartments such as haematopoietic stem cells [13], which give rise to immune cells.

Although the role of $p16^{INK4a}$ in mature immune cells has not yet been investigated, a number of studies has shown that the *CDKN2A* locus is associated with an increased risk for coronary heart disease [14], atherosclerosis [15], and type 2 diabetes (T2D) [16]. In these pathologies, immune cells, such as macrophages, play a crucial role. Besides their pleiotropic immune functions, macrophages also play a role in the development and homeostasis of several tissues, such as adipose tissue [17] and liver [18]. Depending upon the cytokine environment, macrophages differentiate into distinct subclasses with specific characteristics. Classically activated macrophages (CAMϕ) differentiate in presence of Th1 cytokines, such as interferon gamma (IFNγ), or in presence of bacterial products such as lipopolysaccharide (LPS). CAMϕ trigger pro-inflammatory responses required to kill intracellular pathogens [19]. Alternatively activated macrophages (AAMϕ), induced by Th2 cytokines such as interleukin (IL)-4 and IL-13, are associated with Th2-type immune

responses as seen in helminth parasite infections [1]. During inflammation, AAMϕ play a key role in protecting the organism against tissue damage [2]. However, little is known about the mechanisms underlying the acquisition of the AAMϕ phenotype.

In the present study, we investigated whether $p16^{INK4a}$-deficiency influences macrophage activation *in vitro*, using bone marrow-derived macrophages (BMDM), and *in vivo* by infection with the parasite *Schistosoma mansoni.* BMDM from $p16^{INK4a}$-deficient ($p16^{-/-}$) mice exhibit a phenotype resembling IL-4-induced macrophage polarization and an enhanced response to the Th2 cytokine IL-4 compared to BMDM from wild type ($p16^{+/+}$) mice. By contrast, their response to Th1 stimuli is diminished. Moreover, *Schistosoma mansoni* infection of mice transplanted with $p16^{-/-}$ bone marrow resulted in an increased hepatic AAMϕ signature *in vivo*. Finally, we show that $p16^{INK4a}$-deficiency does not influence the IL-4-induced STAT6 pathway. By contrast, the lower response to classical activation stimuli likely occurs through an inhibition of the phosphorylation of both STAT1 and IKKα,β, which correlated with decreased JAK2 phosphorylation and increased acetylation of STAT1 and IKKα,β,

METHODS

Mice. C57BL/6J $p16^{INK4a}$-deficient and littermate control mice on a C57Bl6 background (>97%) were kindly provided by P. Krimpenfort. $p16^{-/-}$ mice showed neither abnormalities in biochemical parameters nor spontaneous tumor development at the studied age. Flow cytometry analysis of splenic T- and B-cells or macrophages showed no differences between $p16^{-/-}$ and $p16^{+/+}$ mice (data not shown). All protocols were conducted with the approval of the Pasteur Institute ethical review board, Lille, France.

Bone marrow chimeras. 8 week-old C57BL/6J mice were lethally irradiated (8 Gy) and injected in the tail vein the next day with $10x10^6$ bone marrow cells isolated from $p16^{-/-}$ or $p16^{+/+}$ donor mice. Mice were supplied with autoclaved acidified water (pH=2) supplemented with neomycin 100 mg/L (Cat.N1142, Sigma-Aldrich), polymyxin B sulphate 60000 U/L (Cat.21850029, Invitrogen) 1 week before and 4 weeks after transplantation. Mice were studied 6 weeks post-transplantation to allow repopulation by the donor bone marrow. To ensure that donor bone marrow replaced the resident blood cell population, DNA was extracted from whole blood with an Illustra blood kit (GE Healthcare). PCR was performed with forward 5'-GCA-GTG-TTG-CAG-TTT-GAA-CCC-3' and reverse 5'-TGT-GGC-AAC-TGA-TTC-AGT-TTG-3' primer sets yielding products of different lengths, which were separated on a 1.5% agarose gel and quantified with the Gel Doc XR system (Bio-Rad). Over 95% of host blood cells were from donor origin.

Primary cell isolation and culture. LPS-elicited neutrophils from air pouches were isolated as described [21]. Splenic $CD4^+$ T-cells and $CD43^-$ B-cells were isolated from female mice respectively using Dynal (Invitrogen), biotin-conjugated anti-CD43 (Becton Dickinson) and streptavidin conjugated to magnetic beads (Miltenyi Biotech) according to manufacturer's instructions. Bone marrow-derived dendritic cells were prepared as described [22]. BMDM were obtained from femoral and tibial bone marrow suspensions, plated at $10x10^6$ cells in 10 cm plates and differentiated in BMDM medium (RPMI 1640 containing Hepes 25 mM

supplemented with 10% low endotoxin fetal bovine serum, 15% L929-conditioned medium, 2 mM L-glutamine, 1 mM gentamycine). Stimulations and microarray analysis were carried out at day 8. IL-4 (15 ng/mL) and IFNγ (2.5 ng/mL and 10 ng/mL) were obtained from Peprotech. LPS (100 ng/mL) from *E. coli* serotype 0111B4 was from Sigma-Aldrich. CINK4 (#219492) was obtained from Merck. For indirect co-culture experiments, conditioned medium of alternatively differentiated $p16^{+/+}$ and $p16^{-/-}$ macrophages was added to cultures of BMDM 24h before LPS (100 ng/mL) stimulation. After 4h, CAMϕ were washed and cultured for 24h in fresh medium. The resulting media were assayed for cytokine secretion by ELISA.

Flow cytometry. During *in vitro* differentiation, asynchronously growing cultures of BMDM were gently scraped every two days with PBS 1X/EDTA 10 mM/2% trypsine, washed with PBS and collected by centrifugation (5 min, 900 rpm). For protein analysis, non-specific staining was avoided by incubating cells with purified rat anti-mouse CD16/CD32 (Cat.553141, BD Pharmingen) for 20 min at 4°C and labeled with anti-mouse F4/80-FITC (Cat.RM2901, Caltag Laboratories) for 30 min at 4°C. Cells were analyzed using a Coulter EPICS XL4-MCL® Flow cytometer (BeckmanCoulter) and Expo32® software (applied cytometry systems). For cell sorting, cells were incubated with anti-mouse F4/80-FITC antibodies (11-4801, eBioscience) and Rat IgG2a K isotype (11-4321, eBioscience) and sorted on an EPICS-ALTRA cell sorter (Beckman Coulter). For FACS-based cell cycle analysis, cells were fixed with 70% ethanol for 1h at -20°C and labeled with 50 µg/mL propidium iodide containing 50 µg/mL RNase A for 30 min at room temperature. The percentage of cell cycle distribution was obtained using the Multicycle® software (Phoenix Flow systems).

Microarray studies. Mouse genome MOE 430 2.0 gene chips (Affymetrix®) were used in triplicate for each condition. Sample preparation, hybridization and scanning were performed according the One-cycle protocol (Affymetrix®). Only genes significantly regulated ($p<0.05$)

were analyzed further with Genomatix Bibliosphere®. Microarray data have been deposited to http://www.ebi.ac.uk/arrayexpress.

RNA extraction and analysis. Total RNA was obtained from BMDM using EXTRACT-ALL®, DNase-I treated, and cDNA was generated using cDNA reverse transcription kit (AB Applied Biosystems). Real-time QPCR detection was conducted on a Stratagene Mx3005P® (Agilent technologies) using Brilliant II SYBR Green reagent® (Agilent Technologies) and specific primers (Table S1). mRNA levels were normalized to 36B4 mRNA and fold induction was calculated using the $2^{-\Delta\Delta Ct}$ method.

Cytokine production measurement. IL-6, TNF, IL-1Rn, IL-4, IL-10 and IFNγ levels in culture supernatants were measured with ELISA kits according to the manufacturer's instructions (R&D systems). Plasma IgE from infected animals was determined by ELISA using purified rat anti-mouse IgE (Cat.553416, BD Pharmingen) as a capture antibody, and biotin rat anti-mouse IgE as a detection antibody (Cat.553414, BD Pharmingen). Standards were prepared using purified mouse IgE κ isotype control (Cat.557079, BD Pharmingen).

Protein extraction and Western blotting. BMDM lysates were prepared using Cell Lysis Buffer (#9803, Cell Signaling Technology) supplemented with 1 mM PMSF. Lysates were resolved in 16% or 10% SDS-PAGE and analyzed by western-blot. Anti-p16 (sc-1207), -actin (sc-1616) and -p38 (sc-535) antibodies were purchased from Santa Cruz Biotechnology. Anti-phospho-STAT6 and -STAT6 (#9361 and 9362), anti-phospho-STAT1 and -STAT1 (#9171 and 9172), anti-phospho-p38 (#9211), anti-phospho-IKKα,β (#2681), anti-IκBα (#9242) and anti-phospho-JAK2 and -JAK2 (#3771 and 3230) antibodies were purchased from Cell Signaling Technology. Hybridizations were done 1:1000 in 5% BSA, 1X TBS, 0.1% Tween-20 overnight at 4°C. Anti-rabbit IgG Peroxidase conjugate secondary antibody 1:10000 (Cat.A-0545, Sigma-Aldrich) was added for 1h at room temperature. Signals were

visualized using the enhanced chemiluminescence Western blot detection kit (Amersham ECL plus Western blotting Detection System; GE Healthcare). Membranes were stripped with Reblot Plus Strong Antibody Stripping Solution® (Cat.2504, Millipore) and re-blotted with the indicated antibodies.

Immunoprecipitation (IP) assay. 500 µg of BMDM lysates were prepared using lysis buffer supplemented with trichostatin A 1 µM (Cat.T8552, Sigma-Aldrich). Lysates were mixed with 100 µL of Protein G/Protein A Agarose (Millipore) and rotated for 1h at 4°C. After centrifugation for 2 min at 3000 rpm, anti-acetyl-Lysine antibody 1:100 (ab21623, Abcam) was added. Samples were rotated overnight at 4°C. The Protein G/Protein A Agarose mix (100 µL) was added to the samples and incubated for 1h at 4°C. The beads were washed 3x and the pellets dissolved in 40 µL of Laemmli 2X buffer. Proteins were analyzed by western blotting as previously described.

***S. mansoni* infection.** Chimeric mice were anesthetized and percutaneously infected with 40 *S. mansoni* cercariae and sacrificed 9 weeks later. The liver was perfused and adult worms were recovered and quantified. A piece of liver was weighed and dissolved in a KOH solution (5%, 37°C during 16h) and eggs were counted. Organs were snap frozen or fixed in paraformaldehyde for further analysis. Resin-embedded livers were cut at 5 µm and Mallory's Trichrome staining was performed to determine granuloma size and hepatic collagen. Immunostaining was performed using antibodies directed to Moma-2 (sc59332, Santa Cruz), Arginase1 (Arg-I) (ab60176-100), Fizz1 (ab39626-50) and Ym1 (ab93034) from Abcam. May Grunwald Giemsa staining was performed and eosinophils were counted per granuloma area. Granulomas were isolated using an Arcturus Laser capture microdissection system from 14 µm sections of snap frozen liver samples. For *ex vivo* restimulation, spleens were homogenized, filtered (70 µm) and erythrocytes were lysed. Cells were cultured in RPMI 1640 (Gibco) supplemented with 10% low endotoxin fetal bovine serum and 1 mM gentamycin. $5x10^5$ cells were stimulated with 10 µg/ml soluble egg antigen (SEA) or anti-

CD3 (#555274; BD Pharmingen) antibodies during 4 days after which medium was collected for cytokine determination by ELISA.

Statistical analysis.

Groups were compared using 2-tailed non-paired *t*-tests using GraphPad Prism® software. *In vitro* data are expressed as means ± SD and *in vivo* data are expressed as means ± SEM.

RESULTS

$p16^{INK4a}$ expression increases during macrophage maturation, but $p16^{INK4a}$-deficiency does not modulate macrophage cell cycle progression.

In order to assess whether and in which mature immune cell types $p16^{INK4a}$ is expressed, $p16^{INK4a}$ mRNA was measured in dendritic cells (DC), bone marrow-derived macrophages (BMDM) and neutrophils, all of myeloid origin, and in B- and T-lymphocytes. $p16^{INK4a}$ was highly expressed in BMDM and DC, while its expression was markedly lower in neutrophils and virtually absent in lymphocytes (Figure 1A). Since the *CDKN2A* locus has been associated to diseases with inflammatory components in which macrophages play a central role, we focused on the role of $p16^{INK4a}$ in these cells. BMDM displayed a gradual increase in $p16^{INK4a}$ mRNA expression during *in vitro* differentiation (Figure 1B). Cell sorting analysis showed that $p16^{INK4a}$ mRNA expression increased specifically in F4/80-positive cells (macrophages) (Figure S1). Together, these data show that increased expression occurs in a higher number of macrophages which also express higher $p16^{INK4a}$ levels. In line, $p16^{INK4a}$ protein was expressed in differentiated macrophages (Figure 1C). Absence of $p16^{INK4a}$ (Figure 1C) did not influence macrophage maturation, since it affected neither mRNA (Figure 1D) nor protein (Figure 1E) expression of the macrophage surface marker F4/80 during differentiation. Interestingly, absence of $p16^{INK4a}$ did not affect cell cycle progression at any time point of *in vitro* macrophage differentiation (Figure 1F). Expression analysis of the INK4 family members $p15^{INK4b}$, $p18^{INK4c}$, $p19^{INK4d}$ and $p19^{ARF}$, another product of the *INK4A/ARF* locus which inhibits the p53 pathway, as well as the KIP/CIP family members $p21^{WAF1}$ and $p27^{KIP1}$ revealed increased expression of $p15^{INK4b}$ in $p16^{INK4a}$-deficient ($p16^{-/-}$) BMDM (Fig. S2). Together with the observation that expression of Cyclin D, a direct E2F target gene, is similar in both genotypes (Figure S3), these data suggest that the induction of $p15^{INK4b}$ may compensate for $p16^{INK4a}$-deficiency in the control of the cell cycle.

These data indicate that $p16^{INK4a}$ expression increases during macrophage differentiation and that $p16^{INK4a}$-deficiency influences neither maturation nor the cell cycle in BMDM.

Macrophage $p16^{INK4a}$-deficiency leads to a phenotype resembling IL-4-induced macrophage polarization.

Microarray analysis of $p16^{-/-}$ BMDM revealed that the expression of a large number of inflammatory genes was significantly lower compared to wild type ($p16^{+/+}$) BMDM under basal conditions (Figure 2A). Several of these genes are typically associated with a CAMϕ phenotype [23-27]. By contrast, a number of AAMϕ-associated genes, linked to IL-4-induced STAT6 activation [23-27], were significantly higher expressed in $p16^{-/-}$ BMDM (Figure 2B). However, the AAMϕ markers Ym1/2 and Fizz1 were not spontaneously induced by $p16^{INK4a}$-deficiency. The differential expression of a number of these genes was confirmed by QPCR (Table S2).

To further characterize this IL-4-like phenotype of $p16^{-/-}$ BMDM, the gene signature of these cells was compared with the gene signature of $p16^{+/+}$ BMDM polarized *in vitro* by addition of IL-4 from day 0 of differentiation, generating $p16^{+/+}$ AAMϕ [28]. Compared to $p16^{+/+}$ BMDM, 14311 probesets were differentially expressed in $p16^{+/+}$ AAMϕ (Figure 2C, green dots), whereas 7605 probesets were regulated in $p16^{-/-}$ BMDM (Figure 2C, red dots), of which the majority (78%) was also differentially expressed in $p16^{+/+}$ AAMϕ (Figure 2C, blue dots). In addition, a strong correlation ($p<0.0001$; Pearson $R=0.7$; $R^2=0.5$) was found between the two experimental conditions (Figure 2C), as also illustrated by a heat map representation of a selection of AAMϕ and CAMϕ marker genes (Figure 2D and Table S3).

Since $p16^{-/-}$ BMDM displayed lower expression levels of inflammatory genes (Figure 2A, D), the secretion of inflammatory cytokines produced in $p16^{-/-}$ BMDM compared to $p16^{+/+}$ BMDM was measured. Under basal conditions, secretion of the pro-inflammatory cytokines IL-6 and TNF was lower (Figure 3A, B) in $p16^{-/-}$ BMDM. By contrast, secretion of anti-inflammatory IL-1Rn was, albeit modestly, higher (Figure 3C). These observations are in line with the microarray data and suggest that $p16^{-/-}$ BMDM are functionally different from their wild type counterparts.

Next, we compared the response of $p16^{-/-}$ *vs.* $p16^{+/+}$ BMDM to polarization into AAMϕ induced by IL-4 added at the start (day 0) of differentiation. Induction of the AAMϕ marker genes Arg-I (Figure 3D) and Ym1/2 (Figure 3E) was higher in $p16^{-/-}$ AAMϕ. However, induction of Mgl2 (Figure 3F) was not different in these cells, suggesting that the IL-4-responsiveness of certain, but not all, genes is dependent on $p16^{INK4a}$. This heterogeneity in regulation of AAMϕ marker genes in IL-4-polarized $p16^{-/-}$ AAMϕ confirms the microarray results (Figure 2D).

Since $p16^{-/-}$ macrophages display increased AAMϕ marker expression after IL-4-induced polarization and since AAMϕ exert paracrine anti-inflammatory effects [29], the functional effects of $p16^{INK4a}$-deficiency on IL-4-induced macrophage polarization were analyzed by indirect co-culture experiments. Hereto, conditioned medium from IL-4-polarized $p16^{-/-}$ or $p16^{+/+}$ AAMϕ was added to $p16^{+/+}$ BMDM and their response to LPS was measured (Figure 3G). Conditioned medium from $p16^{-/-}$ AAMϕ resulted in a more pronounced inhibition of LPS-induced secretion of IL-6 and TNF (Figure 3H, I). Thus, medium from $p16^{-/-}$ AAMϕ more potently inhibits pro-inflammatory responses.

Collectively, these results evidence that $p16^{INK4a}$-deficiency results in a phenotype partially resembling IL-4-induced macrophage polarization. Moreover, IL-4-polarized $p16^{-/-}$ macrophages display a more pronounced AAMϕ phenotype.

$p16^{INK4a}$-deficient macrophages are more responsive to IL-4, while they respond less to IFNγ or LPS.

Since $p16^{-/-}$ BMDM resemble IL-4-polarized macrophages and since $p16^{-/-}$ AAMϕ show more potent anti-inflammatory effects than wild type macrophages, the response of $p16^{-/-}$ BMDM to acute (24h) IL-4 activation was assessed. Interestingly, IL-4 treatment resulted in a larger increase of Arg-I, Ym1/2 and Mgl2 mRNA in $p16^{-/-}$ compared to $p16^{+/+}$ BMDM (Figure 4A-C).

AAMϕ are known to be less sensitive to inflammatory stimuli [19]. Therefore, the effects of IFNγ and LPS, two pro-inflammatory stimuli, were tested on these cells. Interestingly, $p16^{-/-}$ BMDM

were less responsive to IFNγ, shown by the lower induction of the IFNγ target genes iNOS, Cxcl10 and MHCII (Figure 4D-F), as well as to LPS, shown by the decreased response of the LPS-regulated genes TNF, IL-6 and MCP-1 (Figure 4G-I). Expression levels of the cognate receptors for IL-4, IFNγ and LPS was similar in both genotypes (Figure S4A-C), suggesting that the altered responses were not due to differences in receptor expression.

Collectively, these data show that $p16^{-/-}$ BMDM are more responsive to alternative activation by IL-4 and less responsive to the classical macrophage activators IFNγ and LPS.

Haematopoietic $p16^{INK4a}$-deficiency increases hepatic expression of alternatively activated macrophage markers upon *S. mansoni* infection.

Since helminth parasite infections induce a strong Th2 immune response resulting in AAMϕ differentiation [20, 30], the influence of $p16^{INK4a}$-deficiency on macrophage polarization *in vivo* was investigated during *S. mansoni* infection. To assess the role of $p16^{INK4a}$ specifically in haematopoietic cells, $p16^{+/+}$ and $p16^{-/-}$ bone marrow was transplanted in lethally irradiated wild type recipients. Mice were sacrificed 9 weeks after infection, corresponding to the peak of the Th2 immune response, and the hepatic pathology was subsequently characterized.

Expression of Th2 and Th1 cytokines in livers (Figure S5A-D) and spleens (Figure S6A-C), hepatic infection parameters (Table 1), plasma IgE levels (Figure S7), eosinophil infiltration (Table 1), as well as mortality and weight loss (data not shown) did not differ between $p16^{-/-}$ and $p16^{+/+}$ transplanted animals. These results indicate that there are no differences in the lymphocyte-dependent Th2 response, in line with the very low expression of $p16^{INK4a}$ in T-cells (Figure 1A).

Since macrophages express significant levels of $p16^{INK4a}$ (Figure 1A) and since these cells are abundant in *S. mansoni*-induced granulomas [20], macrophage markers were measured in the livers of infected mice. Hepatic mRNA levels of F4/80, CD68 and CD14 were equally induced upon infection (Figure 5A-C), indicating that macrophage numbers were not modified. However, the induction of the AAMϕ markers Ym1/2 (Figure 5D), Fizz1 (Figure 5E)

and Mgl2 (Figure 5F) was higher in mice transplanted with $p16^{-/-}$ *vs.* $p16^{+/+}$ bone marrow. Moreover, expression of the tissue remodeling markers αSMA and Timp1 (Fig. S5E, F) was higher in mice transplanted with $p16^{-/-}$ bone marrow, consistent with the tissue remodeling function of AAMϕ [31].

Immunohistochemical analysis showed that the parasite-induced granulomas are highly macrophage-enriched (Figure S8). Moreover, Arg-I, Fizz1 and Ym1 co-localized with the general macrophage marker Moma-2. Surprisingly, the macrophage population within the granulomas appeared heterogeneous, since these markers did not entirely co-localize (Figure S8). Nevertheless, these data suggest that the increase in hepatic AAMϕ marker expression occurs mainly in macrophages. To unequivocally demonstrate this, the macrophage-positive areas of the granulomas were isolated by laser-capture micro-dissection from $p16^{-/-}$ and $p16^{+/+}$ bone marrow transplanted mice and mRNA levels were measured. $p16^{-/-}$ granulomas displayed increased Mgl2 and Fizz1 mRNA levels, whereas Ym1/2 mRNA tended to be increased (Figure 5G-I). F4/80, CD68 and CD14 expression were identical, indicating that macrophage numbers did not differ between genotypes (data not shown).

Since macrophage polarization influences T-cell activation [20, 32], the *ex vivo* response of splenocytes from mice transplanted with $p16^{+/+}$ or $p16^{-/-}$ bone marrow to soluble *S. mansoni* egg antigen (SEA) was measured. Antigen-independent stimulation of naïve splenocytes by anti-CD3 showed similar IL-4 production (data not shown) suggesting an equal ability of T-cells to synthesize Th2 cytokines, regardless of macrophages within the splenocyte preparation. By contrast, antigen-dependent restimulation with SEA showed a lower production of both IL-4 and IFNγ in splenocytes from $p16^{-/-}$ transplanted mice (Figure S6D, E), while IL-10 production was similar (Figure S6F), hence resulting in an unchanged IL-4/IFNγ balance [33].

Collectively, these results provide evidence for a role of $p16^{INK4a}$ in AAMϕ skewing *in vivo*.

p16^{INK4}-deficiency in macrophages decreases STAT1 and IKKα,β signaling without altering STAT6 phosphorylation.

To unravel the mechanisms underlying the phenotype induced by p16^{INK4a}-deficiency, the microarray data were analyzed to identify which pathways are affected. Interestingly, many genes with a decreased expression in p16$^{-/-}$ BMDM respond to activation of the IFNγ and NF-κB inflammatory signaling pathways (Figure S9), of which STAT1 and IKKα,β respectively are crucial components. Detailed examination of these gene expression patterns revealed that expression levels were comparable (Cxcl10, ifi27, ifi203, ifi47, ifit1, Ccl5, Irak3, Birc3 and Ly6e) or even lower (ifi44, CD55 and NFκBia) in p16$^{-/-}$ BMDM under basal conditions compared to IL-4-polarized p16$^{+/+}$ AAMϕ (Figure 6). Moreover, most inflammatory genes were more strongly inhibited in IL-4-induced p16$^{-/-}$ AAMϕ than in p16$^{+/+}$ AAMϕ (Figure 6 and Figure 2D), suggesting an additive effect of p16^{INK4a}-deficiency on IL-4 treatment. By contrast, such a synergism could not be observed with respect to the AAMϕ marker genes since many of these AAMϕ marker genes responded similarly in IL-4-induced p16$^{-/-}$ and p16$^{+/+}$ AAMϕ (Table S4 and Figure 2D). Collectively, these data show that the pathways controlling IFNγ, NF-κB, and IL-4 signaling are affected by p16^{INK4a}-deficiency in macrophages.

To determine whether the observed differences were related to indirect effects through pRb, BMDM were treated with CINK4, a potent inhibitor of pRb hyperphosphorylation [34]. CINK4 treatment resulted in a dose-dependent decrease of cyclin D mRNA levels both in p16$^{+/+}$ and p16$^{-/-}$ BMDM (Figure S3). Furthermore, treatment with CINK4 in combination with IFNγ did not influence the different phenotype between the two genotypes (Figure S10), thus excluding a role for pRb therein.

STAT6 is the major transcription factor activated by IL-4. Surprisingly, IL-4 treatment induced STAT6 phosphorylation to a similar extent in p16$^{-/-}$ and p16$^{+/+}$ BMDM (Figure 7A). By contrast, IFNγ-induced STAT1 phosphorylation (Figure 7B) and LPS-induced IKKα,β phosphorylation were markedly diminished (Figure 7C) in p16$^{-/-}$ vs. p16$^{+/+}$ BMDM.

Interestingly, IκBα protein levels were increased in $p16^{-/-}$ BMDM under basal conditions (Figure 7C). However, phosphorylation of p38, another downstream target of TLR-4, was not different between $p16^{-/-}$ and $p16^{+/+}$ BMDM (Figure 7C), suggesting that $p16^{INK4a}$-deficiency specifically alters the NF-κB response.

Several genes coding for proteins with acetyl transferase activity were induced in $p16^{-/-}$ BMDM (Table 2). Acetylation of STAT1 and IKKα,β inhibits their phosphorylation and thereby their transcriptional activity [35, 36]. Immunoprecipitation of acetylated proteins revealed that STAT1 and IKKα,β were acetylated to a higher extent in $p16^{-/-}$ than in $p16^{+/+}$ BMDM (Figure 7D). To identify whether STAT1 acetylation is the cause or the consequence of decreased STAT1 phosphorylation, JAK2 phosphorylation, which is upstream in this pathway, was assessed. JAK2 phosphorylation was less pronounced under basal conditions and after activation with IFNγ in $p16^{-/-}$ BMDM (Figure 7E). Since acetylation of STAT1 can interfere with NF-κB signaling [36] and both pathways act synergistically [37], the decreased STAT1 and NF-κB signaling and their increased acetylation probably results from decreased JAK2 phosphorylation.

DISCUSSION

We identify a novel role for the tumor suppressor protein $p16^{INK4a}$ in the regulation of the macrophage phenotype *in vitro* and *in vivo*. $p16^{INK4a}$-deficiency promotes a STAT6-independent IL4-induced macrophage polarization, whereas LPS and IFNγ responses are lower. These actions of $p16^{INK4a}$-deficiency likely occur through modification of the JAK2-STAT1 and NF-κB pathways,

Although $p16^{INK4a}$ is mainly known as a cell cycle inhibitor, cell cycle and macrophage maturation were unaffected in the absence of $p16^{INK4a}$, and an E2F target gene signature[38, 39], which would be expected to be increased by $p16^{INK4a}$-deficiency, could not be identified in $p16^{-/-}$ BMDM. Since $p15^{INK4b}$ is a critical tumor suppressor in the absence of $p16^{INK4a}$ [40] and since an increase of $p15^{INK4b}$ expression was observed in $p16^{-/-}$ BMDM, a compensatory mechanism between these CDKI might have taken place with respect to cell cycle control.

Interestingly, $p16^{INK4a}$ has been previously shown to modulate transcriptional activities of the pro-inflammatory transcription factors NF-κB and AP-1. Via its ankyrin motifs, $p16^{INK4a}$ binds c-jun [41] and NF-κB [42], inhibiting their activity in several immortalized cell lines. However, this mechanism does not appear to play a role in primary murine macrophages, where the loss of $p16^{INK4a}$ has anti-inflammatory effects. Another CDKI, $p21^{WAF1/CIP1}$, was also reported to modulate inflammation without altering cell cycle or differentiation. However, in contrast with $p16^{INK4a}$-deficiency, $p21^{WAF1/CIP1}$-deficiency in macrophages resulted in a higher sensitivity to inflammatory stimuli [43, 44]. Additionally, $p21^{WAF1/CIP1}$ expression was unchanged in $p16^{-/-}$ BMDM.

In a model of AAMϕ differentiation *in vivo*, infection with the helminth *S. mansoni* resulted in equal Th2-associated responses in $p16^{-/-}$ and $p16^{+/+}$ bone marrow transplanted mice. These observations indicate unaltered T-lymphocyte function, in line with the low expression levels of $p16^{INK4a}$ in these cells. By contrast, AAMϕ markers were significantly increased in the livers and in hepatic granulomas of $p16^{-/-}$ bone marrow transplanted animals, probably due to a cell-autonomous activity of $p16^{INK4a}$ in macrophages. Since total bone marrow was

transplanted, a contribution of other haematopoietic cell types to this cell-autonomous macrophage response cannot be excluded. However, since expression of the measured markers was also up-regulated in the macrophage-rich granulomas and since AAMϕ markers co-localized with macrophages in the granuloma, the effects are, at least in part, due to $p16^{INK4a}$-deficiency in the macrophages. Surprisingly, different AAMϕ markers did not strictly co-localize, suggesting the existence of different macrophage populations in defined regions of the granuloma, which could be due to different gradients of stimuli within the granuloma.

Microarray analysis showed that $p16^{-/-}$ BMDM under basal conditions display a gene signature resembling that of IL-4-induced macrophage polarization [27], with the exception of the AAMϕ marker genes Ym1/2 and Fizz1. Moreover, $p16^{-/-}$ BMDM were more responsive to IL-4 activation and displayed weaker pro-inflammatory responses to IFNγ and LPS. Importantly, our data show that $p16^{INK4a}$-deficiency does not influence pRb-mediated activation of the E2F transcription factor. The decreased IFNγ-induced phosphorylation of STAT1 and the LPS-induced IKKα,β phosphorylation in $p16^{-/-}$ BMDM probably account for the attenuated inflammatory responses. Decreased IKKα,β phosphorylation combined with increased IκBα protein levels correlated with the profound decrease of NF-κB target gene expression in $p16^{-/-}$ BMDM. Since a cluster of genes coding for proteins with acetyl transferase activity was induced in $p16^{-/-}$ BMDM and since STAT1 [36] and IKKα,β [35] acetylation reduces their ability to be phosphorylated, the decrease in STAT1 and IKKα,β phosphorylation may result from increased acetylation of these proteins in $p16^{-/-}$ BMDM. The acetylation-phosphorylation balance may be influenced by alterations upstream in the signaling pathway. Since phosphorylation of JAK2, the first component to be phosphorylated upon receptor dimerization [45], was decreased, it appears that the $p16^{INK4a}$-deficiency-induced defect in JAK2 phosphorylation may be implicated in the reduced Stat1 phosphorylation. The increased acetylation status may be a consequence of this mechanism, contributing to the phenotype of $p16^{-/-}$ BMDM. Moreover, JAK2 phosphorylation was less pronounced already under basal culture conditions, in line with the observation that $p16^{INK4a}$-deficiency confers a

lower basal inflammatory phenotype, which is further exacerbated upon stimulation. Since $p16^{INK4a}$-deficiency alters the IFNγ response early in the pathway and TLR4 signaling only at the level of NF-κB, but not, for example, at the level of p38, $p16^{INK4a}$-deficiency thus likely acts directly on the IFNγ and indirectly on the NF-κB signaling pathway.

Surprisingly, STAT6 phosphorylation, the major transcription factor for IL-4-mediated signaling response, was comparable in BMDM of both genotypes, although IL-4-responsive genes were increased in $p16^{-/-}$ BMDM, suggesting that other pathways are involved. It has been shown that STAT1 activation antagonizes expression of STAT6-induced AAMϕ marker genes [46, 47] and that decreased STAT1 phosphorylation can result in an increase of AAMϕ marker genes [48] by a number of molecular mechanisms. First, IL-4 action is inhibited by STAT1 activation through inhibition of STAT6 phosphorylation and its subsequent nuclear translocation in human monocytes [49]. However, $p16^{INK4a}$-deficiency did not modify STAT6 phosphorylation. Second, IFNγ inhibits STAT6 activation by inducing the expression of the suppressor of cytokine signaling 1 (SOCS1) in macrophages [46]. Although SOCS1 mRNA levels were not different between $p16^{-/-}$ and $p16^{+/+}$ BMDM (data not shown), we cannot exclude its involvement via post-transcriptional mechanisms. Third, STAT1 and STAT6 have been shown to compete for binding the same promoters [47], since decreased STAT1 activity increases binding of STAT6 to the promoters of several of its target genes. To our knowledge, an effect of NF-κB signaling on STAT6-dependent gene expression has not yet been demonstrated. Therefore, it is possible that the AAMϕ-like phenotype of $p16^{-/-}$ BMDM is secondary to the decreased CAMϕ-associated response via JAK2-STAT1.

In conclusion, our results identify $p16^{INK4a}$ as a novel modulator of macrophage polarization and show that $p16^{INK4a}$-deficiency skews macrophages towards an IL-4-like phenotype. Since the *CDKN2A* locus is predictive for the risk of T2D and CVD [14, 15], in which macrophage polarization plays a role [28, 50], the role of $p16^{INK4a}$ in the control of macrophage function could be one mechanism contributing to the association of this locus with these diseases.

ACKNOWLEDGMENTS

P.Krimpenfort provided $p16^{INK4a}$-deficient mice. Discussions with G.Raes, J.Vanginderachter and M.de Winther are greatly acknowledged. We thank E.Vallez for mouse breeding, J.Brozek (Genfit SA, Loos, France) for microarray raw data analysis, T.Coevoet , N.Jouy and A.Lucas for technical assistance. This work was supported by the Fondation pour la Recherche Médicale (DCV20070409276 to B.S.), the EFSD/GSK Program 2009, the Cost Action (BM0602) and the Conseil régional Nord Pas-de-Calais and FEDER. C.Cudejko was supported by a doctoral fellowship from the Nouvelle Société Française d'Athérosclérose/Schering-Plough/MSD. K.Wouters was supported by a European FP7 Marie Curie grant (PIEF-GA-2009-235221) and a European Atherosclerosis Society grant.

The funders had no role in study design, data collection and analysis, decision to publish, or preparation of the manuscript.

AUTHORSHIP

C.C. and K.W. designed and performed experiments, analyzed data and wrote the manuscript. L.F., S.A.H., C.P., K.B., E.B., J.V., S.F. and P.R. contributed to some of the experiments. A.T. and G.C contributed to interpret data. D.D., B.S., R.P. contributed to interpretation of the data, manuscript preparation and project supervision. The authors declare no competing financial interests.

ABBREVIATIONS

AAMϕ	Alternatively activated macrophage
BMDM	Bone marrow-derived macrophages
CAMϕ	Classically activated macrophage
CDK	Cyclin-dependent kinase
CDKI	Cyclin-dependent kinase inhibitor
DC	Dendritic cell
IFNγ	Interferon gamma
IL	Interleukin
LPS	Lipopolysaccharide
$p16^{-/-}$	$p16^{INK4a}$-deficient
$p16^{+/+}$	Wild type
QPCR	Quantitative polymerase chain reaction
SEA	Soluble egg antigen
SOCS1	Suppressor of cytokine signaling 1
STAT	Signal transducer and activator of transcription
T2D	Type 2 diabetes

References

[1] Serrano M, Hannon GJ, and Beach D. A new regulatory motif in cell-cycle control causing specific inhibition of cyclin D/CDK4. Nature 1993; 366: 704-7.

[2] Hannon GJ, and Beach D. p15INK4B is a potential effector of TGF-beta-induced cell cycle arrest. Nature 1994; 371: 257-61.

[3] Guan KL, Jenkins CW, Li Y, Nichols MA, Wu X, O'Keefe CL, Matera AG, and Xiong Y. Growth suppression by p18, a p16INK4/MTS1- and p14INK4B/MTS2-related CDK6 inhibitor, correlates with wild-type pRb function. Genes Dev. 1994; 8: 2939-52.

[4] Chan FK, Zhang J, Cheng L, Shapiro DN, and Winoto A. Identification of human and mouse p19, a novel CDK4 and CDK6 inhibitor with homology to p16ink4. Mol. Cell. Biol. 1995; 15: 2682-8.

[5] Hirai H, Roussel MF, Kato JY, Ashmun RA, and Sherr CJ. Novel INK4 proteins, p19 and p18, are specific inhibitors of the cyclin D-dependent kinases CDK4 and CDK6. Mol. Cell. Biol. 1995; 15: 2672-81.

[6] Sharpless NE. INK4a/ARF: a multifunctional tumor suppressor locus. Mutat. Res. 2005; 576: 22-38.

[7] Alcorta DA, Xiong Y, Phelps D, Hannon G, Beach D, and Barrett JC. Involvement of the cyclin-dependent kinase inhibitor p16 (INK4a) in replicative senescence of normal human fibroblasts. Proc. Natl. Acad. Sci. U.S.A. 1996; 93: 13742-7.

[8] Hara E, Smith R, Parry D, Tahara H, Stone S, and Peters G. Regulation of p16CDKN2 expression and its implications for cell immortalization and senescence. Mol. Cell. Biol. 1996; 16: 859-67.

[9] Krishnamurthy J, Torrice C, Ramsey MR, Kovalev GI, Al-Regaiey K, Su L, and Sharpless NE. Ink4a/Arf expression is a biomarker of aging. J. Clin. Invest. 2004; 114: 1299-307.

[10] Nielsen GP, Stemmer-Rachamimov AO, Shaw J, Roy JE, Koh J, and Louis DN. Immunohistochemical survey of p16INK4A expression in normal human adult and infant tissues. Lab. Invest. 1999; 79: 1137-43.

[11] Zindy F, Quelle DE, Roussel MF, and Sherr CJ. Expression of the p16INK4a tumor suppressor versus other INK4 family members during mouse development and aging. Oncogene 1997; 15: 203-11.

[12] Melzer D, Frayling TM, Murray A, Hurst AJ, Harries LW, Song H, Khaw K, Luben R, Surtees PG, Bandinelli SS, Corsi A, Ferrucci L, Guralnik JM, Wallace RB, Hattersley AT, and Pharoah PD. A common variant of the p16(INK4a) genetic region is associated with physical function in older people. Mech. Ageing Dev. 2007; 128: 370-7.

[13] Janzen V, Forkert R, Fleming HE, Saito Y, Waring MT, Dombkowski DM, Cheng T, DePinho RA, Sharpless NE, and Scadden DT. Stem-cell ageing modified by the cyclin-dependent kinase inhibitor p16INK4a. Nature 2006; 443: 421-6.

[14] McPherson R, Pertsemlidis A, Kavaslar N, Stewart A, Roberts R, Cox DR, Hinds DA, Pennacchio LA, Tybjaerg-Hansen A, Folsom AR, Boerwinkle E, Hobbs HH, and Cohen JC. A common allele on chromosome 9 associated with coronary heart disease. Science 2007; 316: 1488-91.

[15] Liu Y, Sanoff HK, Cho H, Burd CE, Torrice C, Mohlke KL, Ibrahim JG, Thomas NE, and Sharpless NE. INK4/ARF transcript expression is associated with chromosome 9p21 variants linked to atherosclerosis. PLoS One 2009; 4: e5027.

[16] Saxena R, Voight BF, Lyssenko V, Burtt NP, de Bakker PIW, Chen H, Roix JJ, Kathiresan S, Hirschhorn JN, Daly MJ, Hughes TE, Groop L, Altshuler D, Almgren P, Florez JC, Meyer J, Ardlie K, Bengtsson Boström K, Isomaa B, Lettre G, Lindblad U, Lyon HN, Melander O, Newton-Cheh C, Nilsson P, Orho-Melander M, Råstam L, Speliotes EK, Taskinen M, Tuomi T, Guiducci C, Berglund A, Carlson J, Gianniny L, Hackett R, Hall L, Holmkvist J, Laurila E, Sjögren M, Sterner M, Surti A, Svensson M, Svensson M, Tewhey R, Blumenstiel B, Parkin M, Defelice M, Barry R, Brodeur W, Camarata J, Chia N, Fava M, Gibbons J, Handsaker B, Healy C, Nguyen K, Gates C, Sougnez C, Gage D, Nizzari M, Gabriel SB, Chirn G, Ma Q, Parikh H, Richardson D, Ricke D, and Purcell S. Genome-wide association analysis identifies loci for type 2 diabetes and triglyceride levels. Science 2007; 316: 1331-6.

[17] Wei S, Lightwood D, Ladyman H, Cross S, Neale H, Griffiths M, Adams R, Marshall D, Lawson A, McKnight AJ, and Stanley ER. Modulation of CSF-1-regulated post-natal development with anti-CSF-1 antibody. Immunobiology 2005; 210: 109-19.

[18] Baffy G. Kupffer cells in non-alcoholic fatty liver disease: the emerging view. J. Hepatol. 2009; 51: 212-23.

[19] Gordon S. Alternative activation of macrophages. Nat. Rev. Immunol. 2003; 3: 23-35.

[20] Herbert DR, Hölscher C, Mohrs M, Arendse B, Schwegmann A, Radwanska M, Leeto M, Kirsch R, Hall P, Mossmann H, Claussen B, Förster I, and Brombacher F. Alternative macrophage activation is essential for survival during schistosomiasis and downmodulates T helper 1 responses and immunopathology. Immunity 2004; 20: 623-35.

[21] Bellosta S, Via D, Canavesi M, Pfister P, Fumagalli R, Paoletti R, and Bernini F. HMG-CoA reductase inhibitors reduce MMP-9 secretion by macrophages. Arterioscler. Thromb. Vasc. Biol. 1998; 18: 1671-8.

[22] Dubois A, Deruytter N, Adams B, Kanda A, Delbauve S, Fleury S, Torres D, François A, Pétein M, Goldman M, Dombrowicz D, and Flamand V. Regulation of Th2 Responses and Allergic Inflammation through Bystander Activation of CD8+ T Lymphocytes in Early Life. J. Immunol. 2010; : .

[23] Van Ginderachter JA, Movahedi K, Hassanzadeh Ghassabeh G, Meerschaut S, Beschin A, Raes G, and De Baetselier P. Classical and alternative activation of mononuclear phagocytes: picking the best of both worlds for tumor promotion. Immunobiology 2006; 211: 487-501.

[24] Vats D, Mukundan L, Odegaard JI, Zhang L, Smith KL, Morel CR, Wagner RA, Greaves DR, Murray PJ, and Chawla A. Oxidative metabolism and PGC-1beta attenuate macrophage-mediated inflammation. Cell Metab 2006; 4: 13-24.

[25] Martinez FO, Gordon S, Locati M, and Mantovani A. Transcriptional profiling of the human monocyte-to-macrophage differentiation and polarization: new molecules and patterns of gene expression. J. Immunol. 2006; 177: 7303-11.

[26] Noël W, Raes G, Hassanzadeh Ghassabeh G, De Baetselier P, and Beschin A. Alternatively activated macrophages during parasite infections. Trends Parasitol. 2004; 20: 126-33.

[27] Mantovani A, Sica A, Sozzani S, Allavena P, Vecchi A, and Locati M. The chemokine system in diverse forms of macrophage activation and polarization. Trends Immunol. 2004; 25: 677-86.

[28] Bouhlel MA, Derudas B, Rigamonti E, Dièvart R, Brozek J, Haulon S, Zawadzki C, Jude B, Torpier G, Marx N, Staels B, and Chinetti-Gbaguidi G. PPARgamma activation primes human monocytes into alternative M2 macrophages with anti-inflammatory properties. Cell Metab 2007; 6: 137-43.

[29] Katakura T, Miyazaki M, Kobayashi M, Herndon DN, and Suzuki F. CCL17 and IL-10 as effectors that enable alternatively activated macrophages to inhibit the generation of classically activated macrophages. J. Immunol. 2004; 172: 1407-13.

[30] Pearce EJ, M Kane C, Sun J, J Taylor J, McKee AS, and Cervi L. Th2 response polarization during infection with the helminth parasite Schistosoma mansoni. Immunol. Rev. 2004; 201: 117-26.

[31] Wynn TA. Fibrotic disease and the T(H)1/T(H)2 paradigm. Nat. Rev. Immunol. 2004; 4: 583-94.

[32] Elliott DE, and Boros DL. Schistosome egg antigen(s) presentation and regulatory activity by macrophages isolated from vigorous or immunomodulated liver granulomas of Schistosoma mansoni-infected mice. J. Immunol. 1984; 132: 1506-10.

[33] Mosmann TR, and Coffman RL. TH1 and TH2 cells: different patterns of lymphokine secretion lead to different functional properties. Annu. Rev. Immunol. 1989; 7: 145-73.

[34] Soni R, O'Reilly T, Furet P, Muller L, Stephan C, Zumstein-Mecker S, Fretz H, Fabbro D, and Chaudhuri B. Selective in vivo and in vitro effects of a small molecule inhibitor of cyclin-dependent kinase 4. J. Natl. Cancer Inst. 2001; 93: 436-46.

[35] Mittal R, Peak-Chew S, and McMahon HT. Acetylation of MEK2 and I kappa B kinase (IKK) activation loop residues by YopJ inhibits signaling. Proc. Natl. Acad. Sci. U.S.A. 2006; 103: 18574-9.

[36] Krämer OH, Baus D, Knauer SK, Stein S, Jäger E, Stauber RH, Grez M, Pfitzner E, and Heinzel T. Acetylation of Stat1 modulates NF-kappaB activity. Genes Dev. 2006; 20: 473-85.

[37] Hiroi M, and Ohmori Y. The transcriptional coactivator CREB-binding protein cooperates with STAT1 and NF-kappa B for synergistic transcriptional activation of the CXC ligand 9/monokine induced by interferon-gamma gene. J. Biol. Chem. 2003; 278: 651-60.

[38] Vernell R, Helin K, and Müller H. Identification of target genes of the p16INK4A-pRB-E2F pathway. J. Biol. Chem. 2003; 278: 46124-37.

[39] Stanelle J, Stiewe T, Theseling CC, Peter M, and Pützer BM. Gene expression changes in response to E2F1 activation. Nucleic Acids Res. 2002; 30: 1859-67.

[40] Krimpenfort P, Ijpenberg A, Song J, van der Valk M, Nawijn M, Zevenhoven J, and Berns A. p15Ink4b is a critical tumour suppressor in the absence of p16Ink4a. Nature 2007; 448: 943-6.

[41] Choi BY, Choi HS, Ko K, Cho Y, Zhu F, Kang BS, Ermakova SP, Ma W, Bode AM, and Dong Z. The tumor suppressor p16(INK4a) prevents cell transformation through inhibition of c-Jun phosphorylation and AP-1 activity. Nat. Struct. Mol. Biol. 2005; 12: 699-707.

[42] Wolff B, and Naumann M. INK4 cell cycle inhibitors direct transcriptional inactivation of NF-kappaB. Oncogene 1999; 18: 2663-6.

[43] Scatizzi JC, Mavers M, Hutcheson J, Young B, Shi B, Pope RM, Ruderman EM, Samways DSK, Corbett JA, Egan TM, and Perlman H. The CDK domain of p21 is a suppressor of IL-1beta-mediated inflammation in activated macrophages. Eur. J. Immunol. 2009; 39: 820-5.

[44] Trakala M, Arias CF, García MI, Moreno-Ortiz MC, Tsilingiri K, Fernández PJ, Mellado M, Díaz-Meco MT, Moscat J, Serrano M, Martínez-A C, and Balomenos D.

Regulation of macrophage activation and septic shock susceptibility via p21(WAF1/CIP1). Eur. J. Immunol. 2009; 39: 810-9.

[45] Shuai K, and Liu B. Regulation of JAK-STAT signalling in the immune system. Nat. Rev. Immunol. 2003; 3: 900-11.

[46] Dickensheets HL, Venkataraman C, Schindler U, and Donnelly RP. Interferons inhibit activation of STAT6 by interleukin 4 in human monocytes by inducing SOCS-1 gene expression. Proc. Natl. Acad. Sci. U.S.A. 1999; 96: 10800-5.

[47] Ohmori Y, and Hamilton TA. IL-4-induced STAT6 suppresses IFN-gamma-stimulated STAT1-dependent transcription in mouse macrophages. J. Immunol. 1997; 159: 5474-82.

[48] Porta C, Rimoldi M, Raes G, Brys L, Ghezzi P, Di Liberto D, Dieli F, Ghisletti S, Natoli G, De Baetselier P, Mantovani A, and Sica A. Tolerance and M2 (alternative) macrophage polarization are related processes orchestrated by p50 nuclear factor kappaB. Proc. Natl. Acad. Sci. U.S.A. 2009; 106: 14978-83.

[49] Dickensheets HL, and Donnelly RP. Inhibition of IL-4-inducible gene expression in human monocytes by type I and type II interferons. J. Leukoc. Biol. 1999; 65: 307-12.

[50] Odegaard JI, Ricardo-Gonzalez RR, Goforth MH, Morel CR, Subramanian V, Mukundan L, Red Eagle A, Vats D, Brombacher F, Ferrante AW, and Chawla A. Macrophage-specific PPARgamma controls alternative activation and improves insulin resistance. Nature 2007; 447: 1116-20.

TABLES

Table 1. Liver pathology during Schistosomiasis

Parameter	$p16^{-/-}$ donor	$p16^{+/+}$ donor
Male and female worm number	5±1 / 5±1	7±1 / 6±1
Parasite burden (egg number/female/g tissue)	1604±191	1698±359
AST plasma concentration (U/ml)	131±59	115±37
Granuloma number per mm^2 liver area	25±2	28±2
Granuloma area / liver area (mm^2/mm^2)	0.078±0.006	0.087±0.009
Eosinophils / granuloma area (mm^2)	12±1	10±1
Collagen area / liver area	0.132±0.023	0.112±0.014

Table 2. Genes coding for proteins with acetyl transferase activity in $p16^{INK4a}$-deficient macrophages

Probeset	Symbol	Description	fold change	p value
1435224_at	CBP/p300	CREB binding protein	1.96	1,00E-04
1426783_at	Gcn5l2	GCN5 general control of amino acid synthesis-like 2	1.91	2,20E-04
1448711_at	Mcm3ap	minichromosome maintenance deficient 3 associated protein	1.55	8,90E-03
1433692_at	Nat10	N-acetyltransferase 10	1.65	1,80E-04
1419213_at	Nat6	N-acetyltransferase 6	2.11	8,40E-06
1435842_at	Nat8l	N-acetyltransferase 8-like	1.32	4,60E-02
1436580_at	Hgsnat	Heparan-alpha-glucosaminide N-acetyltransferase	1.38	1,80E-02

FIGURE LEGENDS

Figure 1. $p16^{INK4a}$ is expressed, but does not influence maturation or the cell cycle in macrophages.

(**A**) $p16^{INK4a}$ mRNA expression was measured in immune cells isolated from mice: dendritic cells (DC), bone marrow derived-macrophages (BMDM), neutrophils, B-lymphocytes and T-lymphocytes. (**B**) $p16^{INK4a}$ mRNA expression was measured at different stages during differentiation of BMDM isolated from $p16^{+/+}$ mice. Since $p16^{INK4a}$ fold induction differs between experiments, data is from one of three distinct experiments. (**C**) $p16^{INK4a}$ protein expression in $p16^{+/+}$ and $p16^{-/-}$ BMDM was analyzed by Western blot with an anti-$p16^{INK4a}$ antibody. Anti-actin antibody was used as loading control. (**D and E**) Increase of the macrophage marker F4/80 mRNA expression (**D**) and protein expression (**E**) measured by respectively QPCR and flow cytometry in $p16^{+/+}$ and $p16^{-/-}$ BMDM. Data are shown from one of three independent experiments. (**F**) Cell cycle analysis by propidium iodide staining of $p16^{+/+}$ and $p16^{-/-}$ BMDM during differentiation expressed in % of events ± standard deviation.

Figure 2. $p16^{INK4a}$-deficiency induces a gene expression profile resembling IL-4-induced macrophage polarization.

Microarray analysis using mRNA from $p16^{-/-}$ BMDM compared to $p16^{+/+}$ BMDM showed (**A**) decreased mRNA expression of classically activated macrophages-associated genes and (**B**) increased mRNA expression of alternatively activated macrophages-associated genes. Data is expressed as fold change relative to $p16^{+/+}$ BMDM. (**C**) Differential gene expression in $p16^{-/-}$ BMDM relative to $p16^{+/+}$ BMDM was correlated with the changes induced in IL-4-induced $p16^{+/+}$ AAMϕ. The figure shows 2log values of the probesets significantly ($p<0.05$) regulated only in $p16^{-/-}$ BMDM (red dots), only in IL-4-polarized $p16^{+/+}$ AAMϕ (green dots) and by both conditions (blue dots), compared to $p16^{+/+}$ BMDM. The X-axis represents differences in gene expression induced by IL-4, whereas the Y-axis represents the effect of $p16^{INKa}$-deficiency. These comparisons are depicted in the schematic representation of the protocol in the corresponding colors. Pearson Correlation analysis was done for probesets

differentially expressed by both conditions (blue). (**D**) Heat map of $p16^{+/+}$ BMDM, $p16^{-/-}$ BMDM, IL-4-polarized $p16^{+/+}$ and $p16^{-/-}$ AAMϕ gene expression profiles. Colors fluctuate from blue (poorly expressed) to green (intermediate expression) and yellow (high expression). Additional information regarding gene description, fold induction, and p-value can be found in Table S3.

Figure 3. $p16^{INK4a}$-deficient macrophages phenotypically and functionally resemble IL-4-polarized alternatively activated macrophages.

Protein secretion of IL-6 (**A**), TNF (**B**), and IL-1Rn (**C**) was measured in the culture medium of $p16^{+/+}$ and $p16^{-/-}$ BMDM by ELISA. (**D-F**) QPCR analysis of Arg-I (**D**), Ym1/2 (**E**), and Mgl2 (**F**) of $p16^{+/+}$ and $p16^{-/-}$ AAMϕ polarized by addition of 15 ng/mL IL-4 from day 0 of differentiation. (**G**) Schematic representation of the indirect co-culture experiment. (**H and I**) LPS-induced secretion of IL-6 (**H**), and TNF (**I**) was determined by ELISA in $p16^{+/+}$ BMDM supernatants resulting from indirect co-culture. Statistically significant differences are indicated (*t*-test; ***$p<0.001$ **$p<0.01$, and *$p<0.05$).

Figure 4. $p16^{INK4a}$-deficiency modulates macrophage responses to alternatively and classically polarizing stimuli.

mRNA expression from $p16^{+/+}$ and $p16^{-/-}$ BMDM activated with 15 ng/mL IL-4 during 24h (**A-C**), 10 ng/mL IFNγ during 12h (**D-F**), or 100 ng/mL LPS during 2h (**G**) or 24h (**H and I**). mRNA expression of the IL-4-induced target genes Arg-I (**A**), Ym1/2 (**B**), and Mgl2 (**C**); IFNγ-induced target genes iNOS (**D**), Cxcl10 (**E**), and MHCII (**F**); and LPS-induced target genes TNF (**G**), IL-6 (**H**), and MCP-1 (**I**) was quantified by QPCR and expressed as fold increase compared with respective controls. Statistically significant differences are indicated (*t*-test; ***$p<0.001$ **$p<0.01$, and *$p<0.05$).

Figure 5. Haematopoietic deficiency of $p16^{INK4a}$ exacerbates hepatic alternative macrophage activation of *S. mansoni*-infected mice.

Hepatic mRNA expression from mice transplanted with either $p16^{+/+}$ or $p16^{-/-}$ bone marrow which were not infected (naive) or infected with *S. mansoni*, 9 weeks post-infection. mRNA expression of the macrophage markers F4/80 (**A**), CD68 (**B**), and CD14 (**C**); AAMϕ markers Ym1/2 (**D**), Fizz1 (**E**), and Mgl2 (**F**) was quantified by QPCR and expressed as fold increase compared to their respective naive controls. Data was obtained from *n*=10 naive and *n*=14 infected mice per genotype. Hepatic granulomas were isolated by laser-capture microdissection and mRNA expression of the AAMϕ markers Ym1/2 (**G**), Fizz1 (**H**), and Mgl2 (**I**) was quantified by QPCR. Statistically significant differences are indicated (*t*-test; **$p<0.01$ and *$p<0.05$).

Figure 6. $p16^{INK4a}$-deficiency results in an alteration of STAT1 and NF-κB signaling.

Representation of the relative microarray intensity values from a selection of down-regulated genes in $p16^{+/+}$ and $p16^{-/-}$ BMDM with or without polarization (AAMϕ) by 15 ng/mL IL-4 from day 0 of differentiation. Statistically significant differences are indicated (a: $p<0.05$ compared to $p16^{+/+}$ BMDM; b: $p<0.05$ compared to $p16^{-/-}$ BMDM; c: $p<0.05$ compared to $p16^{+/+}$ AAMϕ.)

Figure 7. $p16^{INK4a}$-deficiency diminishes JAK2-STAT1 and NF-κB signaling and increases acetylation of STAT1 and IKKα,β.

Total protein extracts of $p16^{+/+}$ and $p16^{-/-}$ BMDM treated with 15 ng/mL IL-4 (**A**), 2.5 ng/mL IFNγ (**B**) and (**E**), and 100 ng/mL LPS (**C**) for the times indicated. Western blots were performed with the indicated antibodies. (**D**) Total protein extracts from $p16^{+/+}$ and $p16^{-/-}$ BMDM treated with 2.5 ng/mL IFNγ for 5h were then immunoprecipated (IP) with an anti-Acetyl-Lys antibody and then immunoblotted with an anti-STAT1 antibody or with an anti-IKKα,β antibody, as indicated. Input corresponds to 5% of total protein extract used for IP.

Cudejko-Wouters Fig 1

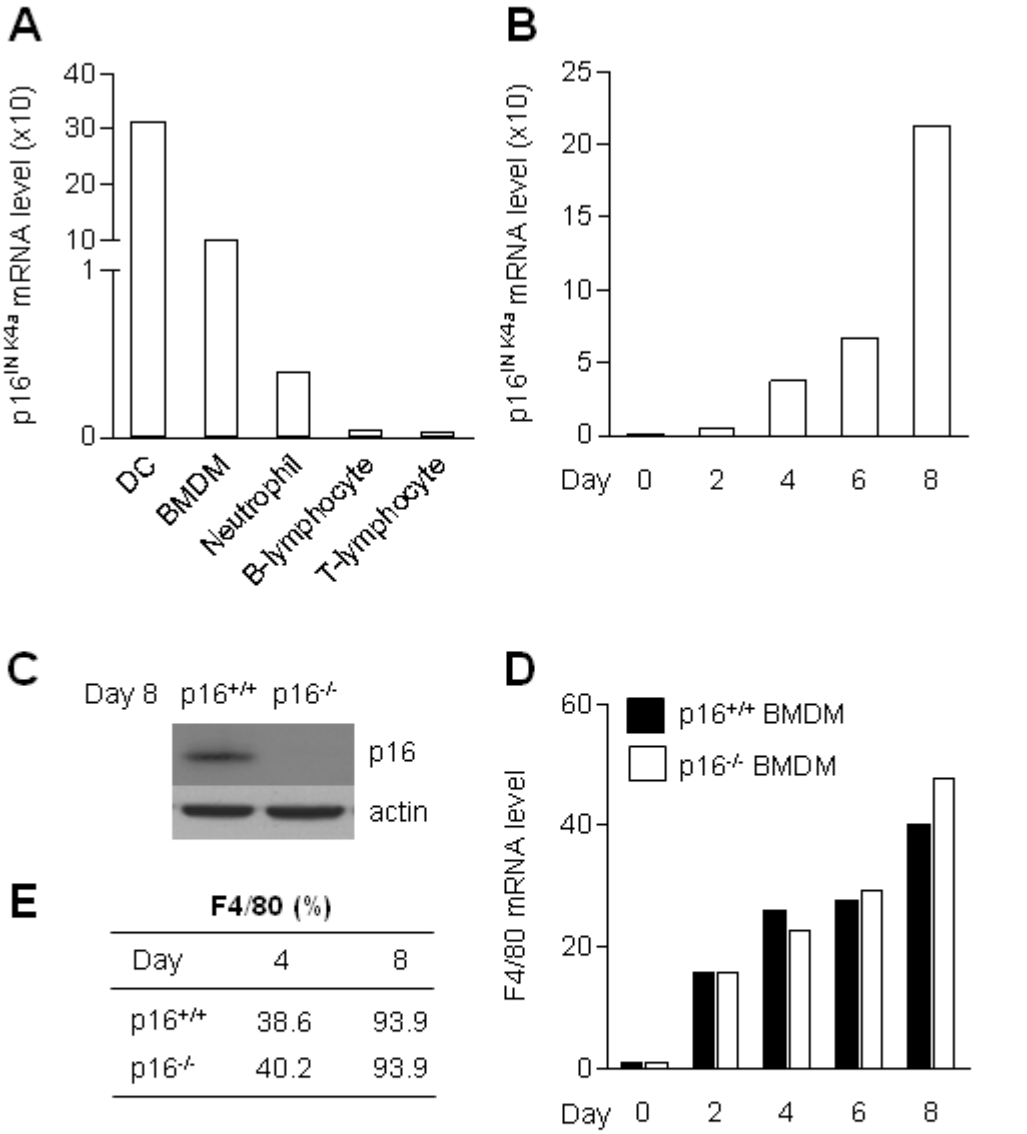

E

F4/80 (%)		
Day	4	8
$p16^{+/+}$	38.6	93.9
$p16^{-/-}$	40.2	93.9

F

Day	0			4			6			8		
	%G1	%S	%G2	%G1	%S	%G2	%G1	%S	%G2	%G1	%S	%G2
$p16^{+/+}$	82.5 ±0.6	7.0 ±0.4	9.6 ±0.9	76.0 ±1.8	10.2 ±1.2	13.1 ±0.9	91.5 ±1.5	3.9 ±0.6	3.4 ±0.5	87.9 ±4.1	6.8 ±2.7	4.5 ±1.6
$p16^{-/-}$	84.3 ±0.1	6.5 ±0.1	8.8 ±0.1	77.3 ±0.7	9.1 ±0.2	12.4 ±0.5	93.0 ±1.7	2.3 ±1.0	3.3 ±0.6	88.5 ±1.1	4.4 ±0.3	3.1 ±0.5

Cudejko-Wouters Fig 2

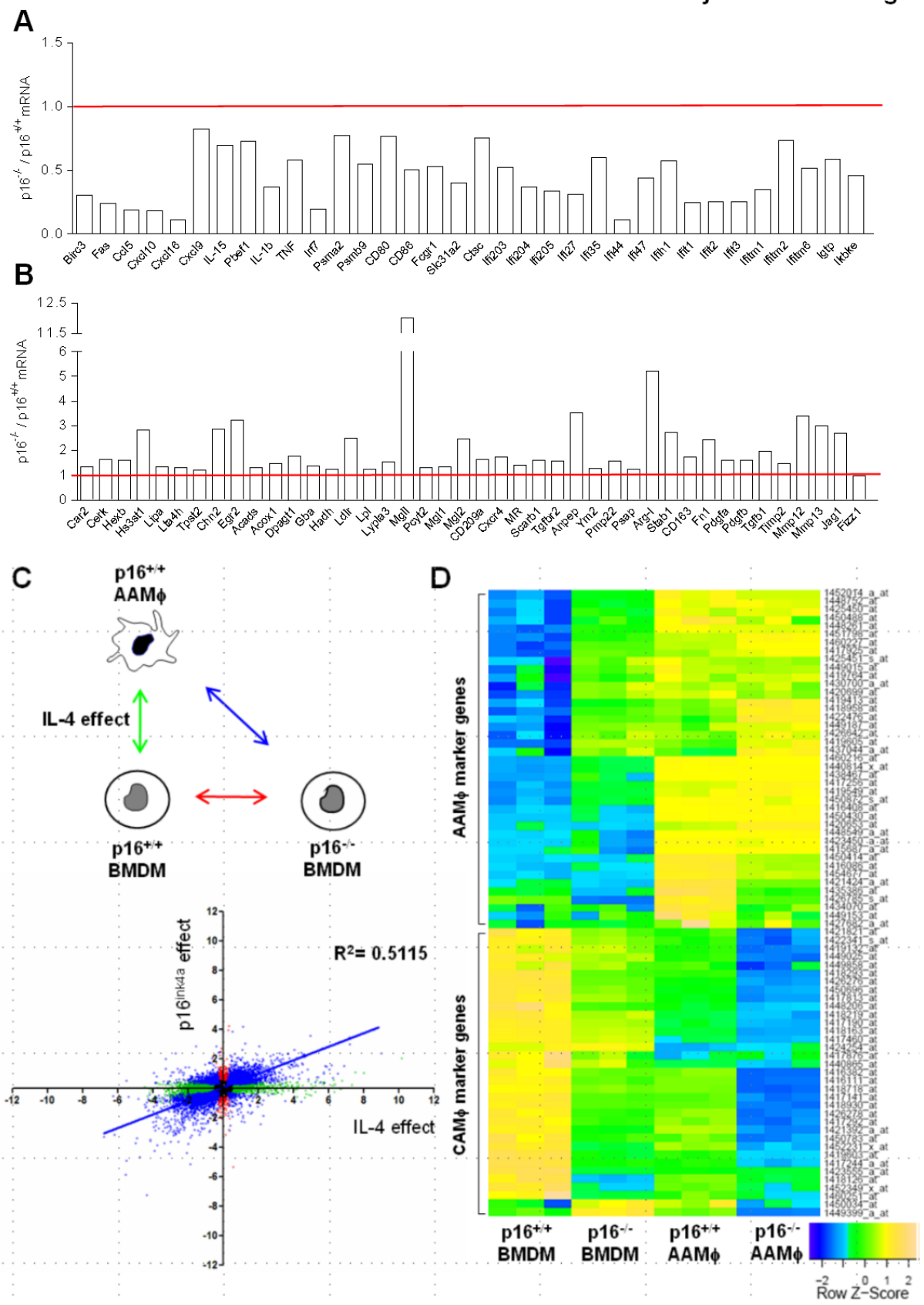

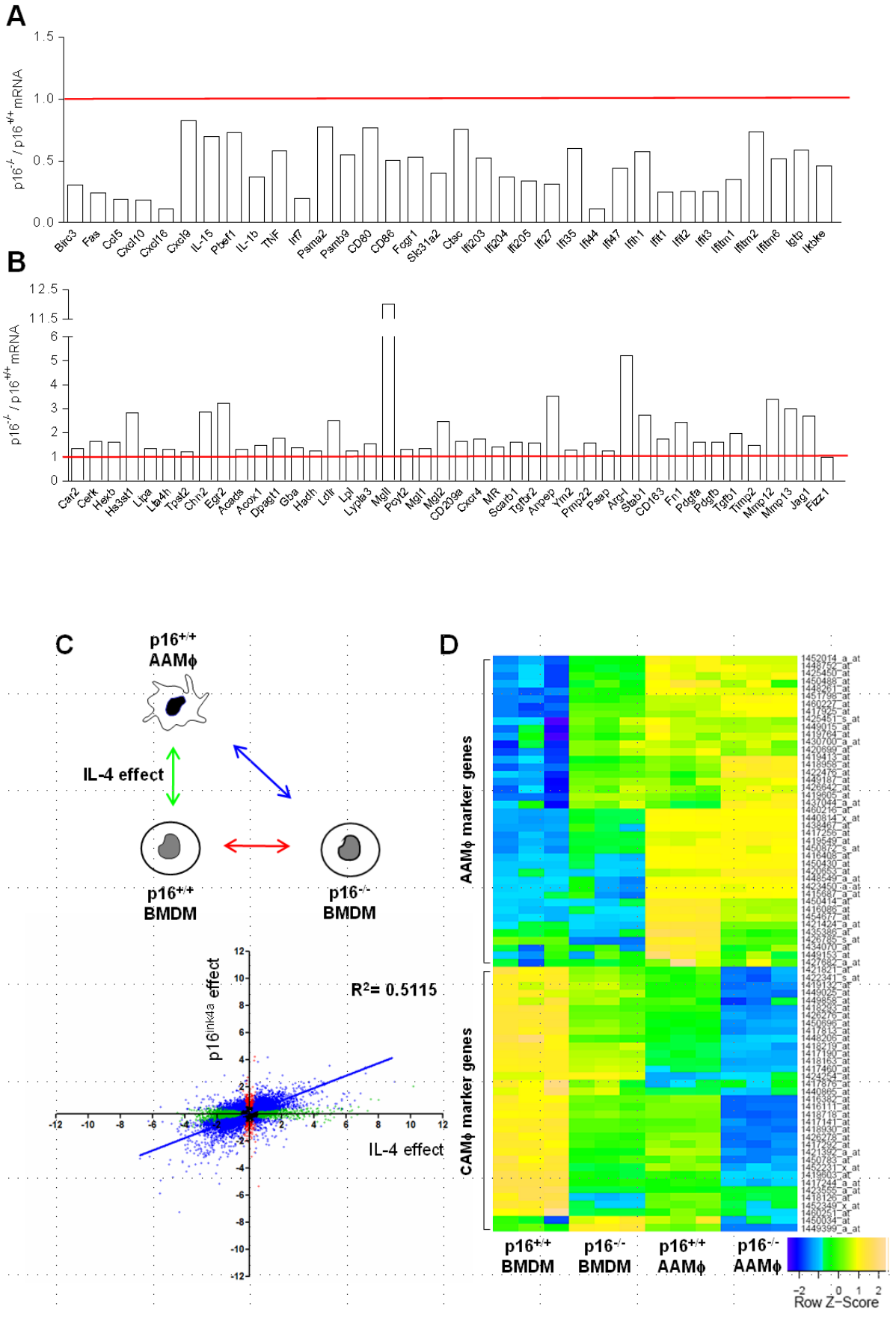
A
p16-/- / p16+/+ mRNA
1.5
1.0
0.5
0.0
Birc3 Fas Ccl5 Cxcl10 Cxcl16 Cxcl9 IL-15 Pbef1 IL-1b TNF Irf7 Psma2 Psmb9 CD80 CD86 Fcgr1 Slc31a2 Ctsc Ifi203 Ifi204 Ifi205 Ifi27 Ifi35 Ifi44 Ifi47 Ifih1 Ifit1 Ifit2 Ifit3 Ifitm1 Ifitm2 Ifitm3 Igtp Ikbke
B
p16-/- / p16+/+ mRNA
12.5
11.5
6
5
4
3
2
1
0
Car2 Cerk Hexb Hs3st1 Lipa Lta4h Tpst2 Chn2 Egr2 Acads Acox1 Dpagt1 Gba Hadh Ldlr Lpl Lypla3 Mgll Pcyt2 Mgl1 Mgl2 CD209a Cxcr4 MR Scarb1 Tgfbr2 Anpep Ym2 Pmp22 Psap Arg1 Stab1 CD163 Fn1 Pdgfa Pdgfb Tgfb1 Timp2 Mmp12 Mmp13 Jag1 Fizz1
C
p16+/+ AAMϕ
IL-4 effect
p16+/+ BMDM
p16-/- BMDM
p16Ink4a effect
R2= 0.5115
IL-4 effect
D
AAMϕ marker genes
CAMϕ marker genes
p16+/+ BMDM
p16-/- BMDM
p16+/+ AAMϕ
p16-/- AAMϕ
Row Z-Score

Cudejko-Wouters Fig 3

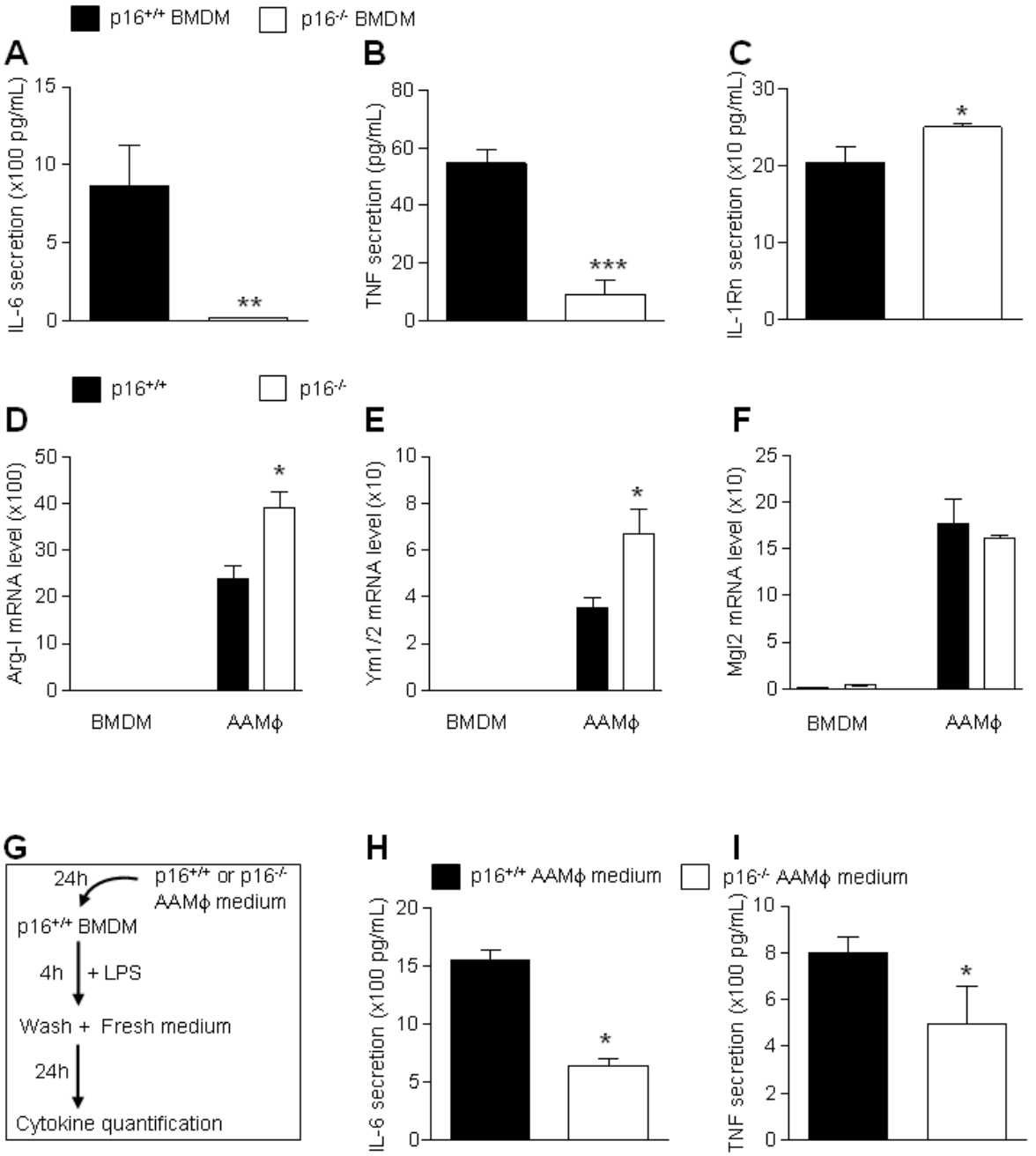

Cudejko-Wouters Fig 4

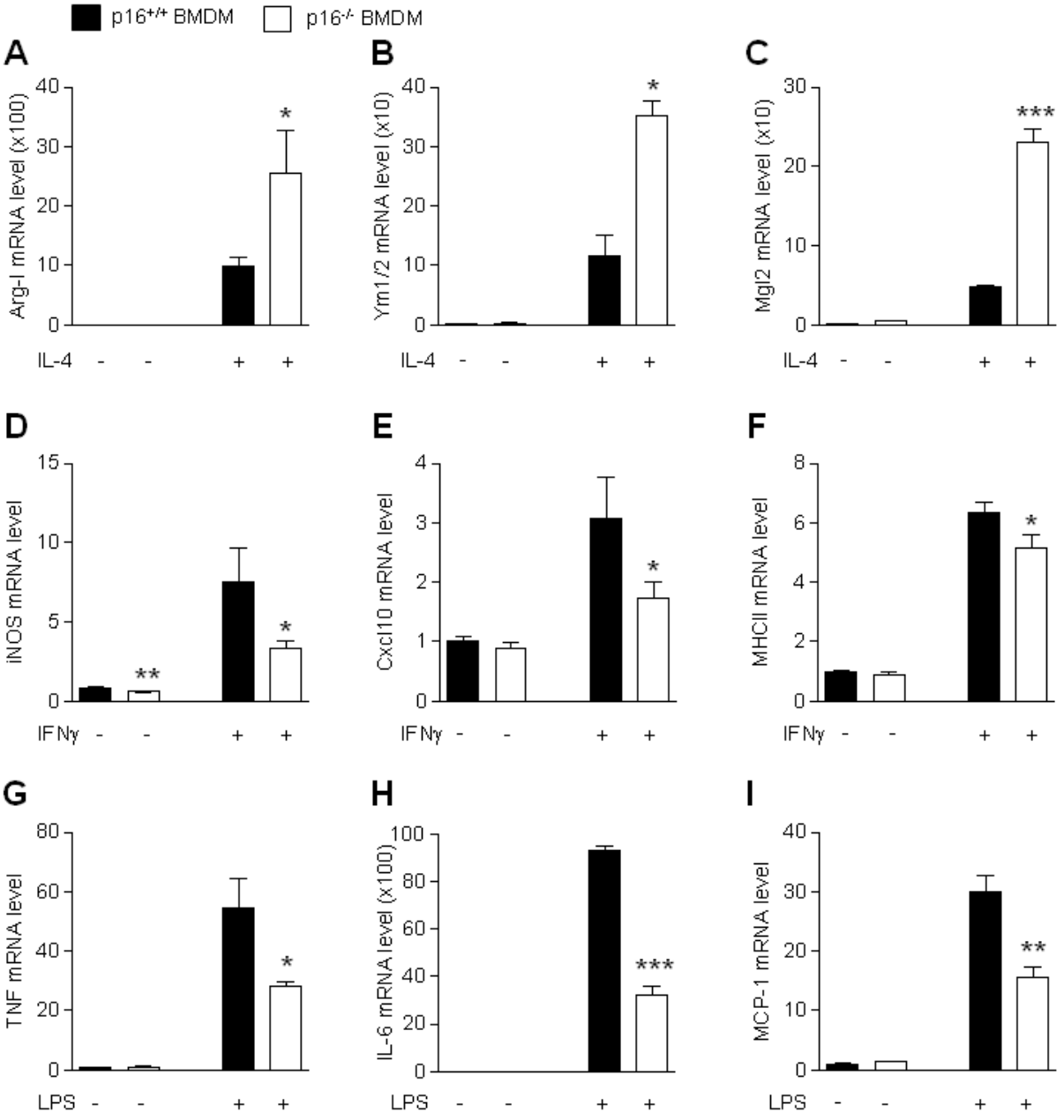

Cudejko-Wouters Fig 5

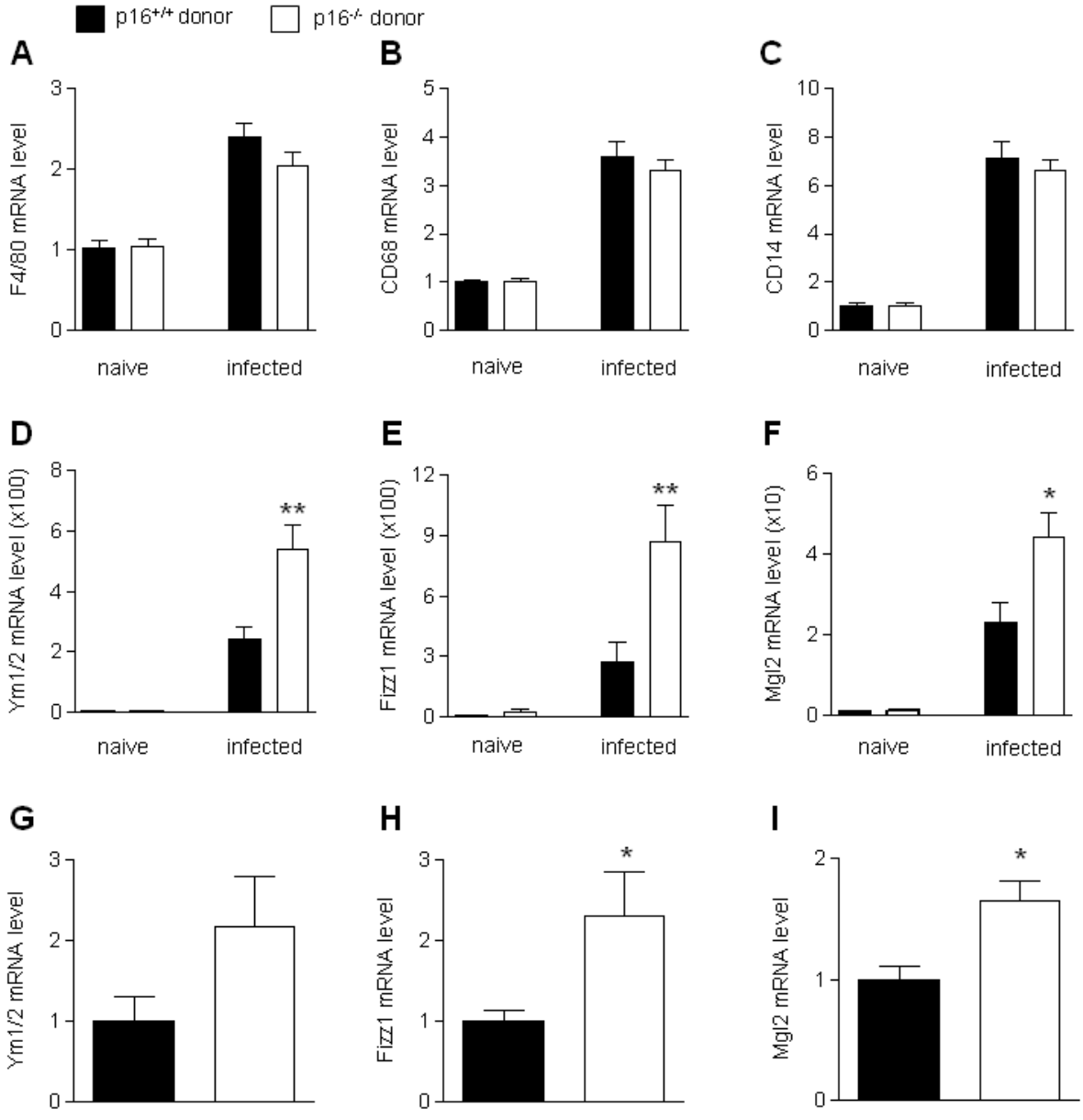

Cudejko-Wouters Fig 6

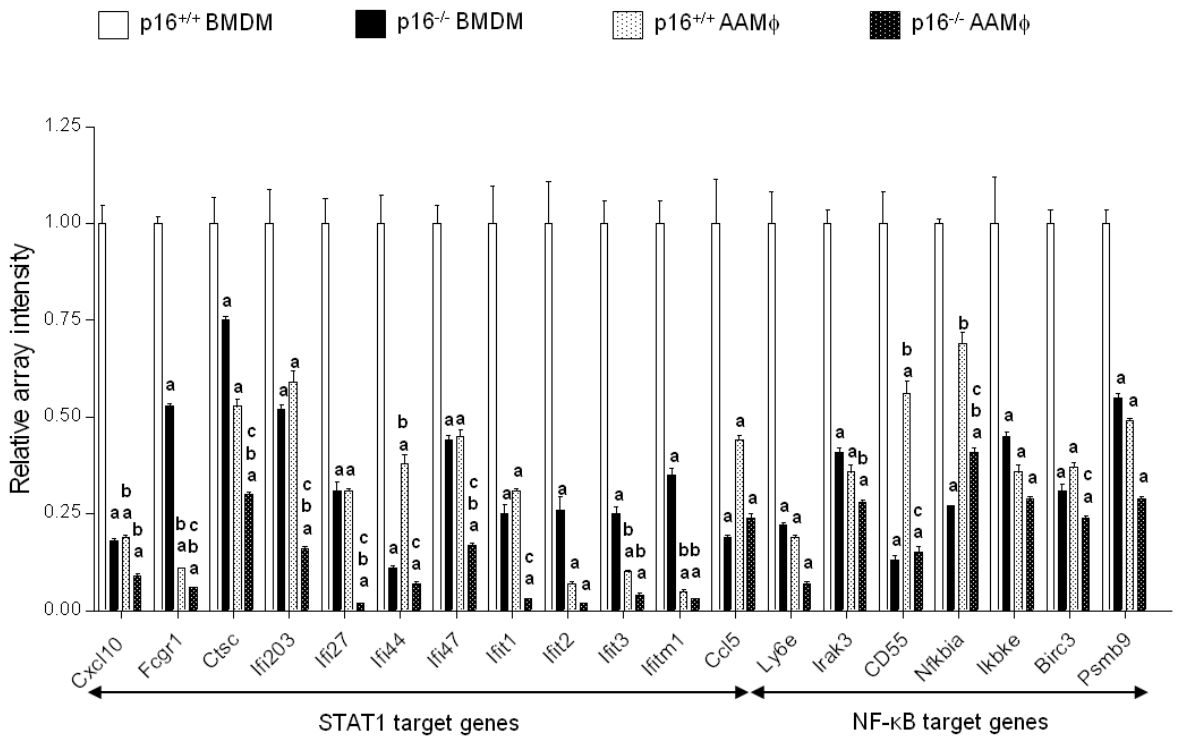
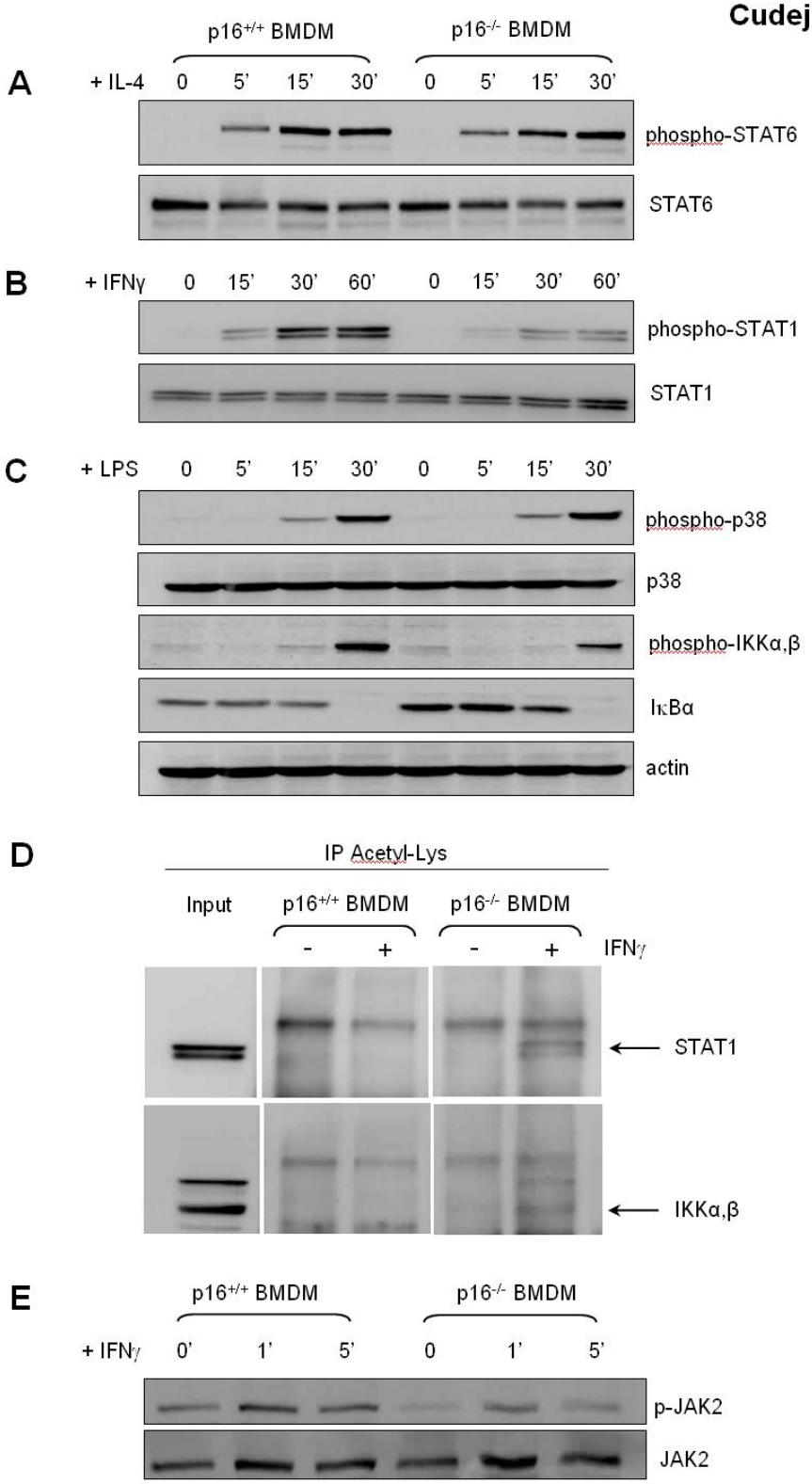
Cudejko-Wouters Fig 7